Increasing Compound Hazards of Tropical Cyclones and Heatwaves over Southeastern Coast of China under Climate Warming

PINYA WANG,[a,e] YANG YANG,[a] DAOKAI XUE,[b] YI QU,[c] JIANPING TANG,[b] L. RUBY LEUNG,[d] AND HONG LIAO[a]

[a] *Jiangsu Key Laboratory of Atmospheric Environment Monitoring and Pollution Control, Jiangsu Collaborative Innovation Center of Atmospheric Environment and Equipment Technology, School of Environmental Science and Engineering, Nanjing University of Information Science and Technology, Nanjing, Jiangsu, China*
[b] *School of Atmospheric Sciences, Nanjing University, Nanjing, Jiangsu, China*
[c] *Institute of Urban Meteorology, China Meteorological Administration, Beijing, China*
[d] *Atmospheric Sciences and Global Change Division, Pacific Northwest National Laboratory, Richland, Washington*
[e] *Nanjing Xinda Institute of Safety and Emergency Management, Nanjing, Jiangsu, China*

(Manuscript received 21 April 2022, in final form 27 October 2022)

ABSTRACT: Compound hazards are more destructive than the individual ones. Using observational and reanalysis datasets during 1960–2019, this study shows a remarkable concurrent relationship between extreme heatwaves (HWs) over southeastern coast of China (SECC) and tropical cyclone (TC) activities over western North Pacific (WNP). Overall, 70% of HWs co-occurred with TC activities (TC–HWs) in the past 60 years. Although the total frequency of TCs over WNP exhibited a decreasing trend, the occurrences of TC–HWs over SECC have been increasing, primarily due to the increasing HWs in the warming climate. In addition, TC–HWs are stronger and longer lasting than HWs that occur alone (AHWs). And in the long-term perspective, both AHWs and TC–HWs exhibit increasing trends, especially since the mid-1980s. The enhancement on HWs caused by TC activities is sustained until TCs make their landfalls and then collapse. Based on composite analysis, TC activities enhance HWs by modulating atmospheric circulations and triggering anomalous descending motion over southern China mainland which intensifies the western Pacific subtropical high (WPSH) and favors increased temperatures therein. Given the severe adverse impacts of TC–HWs on coastal populations, more research is needed to assess the future projections of TC–HWs, as HWs are expected to be more frequent and stronger as the climate warms, whereas TCs over WNP may occur less often.

KEYWORDS: Atmosphere-ocean interaction; Extreme events; Heat wave; Tropical cyclones

1. Introduction

A heatwave (HW) is a period of consecutive extreme high near-surface air temperatures, which is one of the most deadly climate hazards. Many regions across the world have experienced deadly heatwaves in recent decades. For instance, the 2003 heatwaves over Europe lasted for more than one month and caused more than 35 000 deaths (Feudale and Shukla 2011). A devastating heatwave struck Russia in 2010 and caused adverse impacts surpassing the amplitude and spatial extent of the previous hottest summer of 2003 in Europe (Barriopedro et al. 2011). Major heatwaves hit Sichuan basin and central-eastern China in 2006 and 2013, which led to substantial mortality and economic loss (Wang et al. 2016). In summer 2021, the devastating heatwave in western North America lasted from late June to mid-July with exceptionally high air temperature around 50°C far beyond the historical records, which has been attributed to human-caused climate warming (WWA 2021). It is worth noting that high humidity would worsen the negative impacts of excessive heat on human suffering and eventually cause increased mortality rates. The human body has difficulty sweating under extremely humid and heated situations. The buildup of ambient and metabolic heat in the body can lead to medical problems and even death (Budd 2008; P. Wang et al. 2019). Heat stress, generally defined with wet-bulb temperatures, which combine both air temperatures and humidity, is an efficient and widely used measure to assess heat-related mortality rates (e.g., Sherwood and Huber 2010; Kovats and Hajat 2008; Borden and Cutter 2008; Yao et al. 2022).

The global mean surface temperature is now warmer than ever before (IPCC 2021). The successively warmer climate has caused a surge in HWs in the past decades. For example, the frequency, total duration, and maximum duration of heatwaves over central and northwestern India increased during 1961–2013 (Rohini et al. 2016). Such enhancements in heatwaves are also obvious over North America (Wu et al. 2012). Based on observed air temperature, Wang et al. (2017, 2018a) revealed an increasing trend of the magnitude, duration and frequency of heatwaves over China during 1959–2013. Moreover, global warming will exacerbate heatwaves by increasing the frequency and severity in the future. Based on Coupled Model Intercomparison Project phase 5 (CMIP5) outputs, Wang et al. (2018b, 2021) projected that heatwaves in China would become more frequent, longer lasting and stronger, and more areas will face such extreme hot weathers in the coming decades under the representative concentration pathway 8.5 (RCP8.5) scenario.

Supplemental information related to this paper is available at the Journals Online website: https://doi.org/10.1175/JCLI-D-22-0279.s1.

Corresponding author: Y. Yang, yang.yang@nuist.edu.cn

DOI: 10.1175/JCLI-D-22-0279.1

A tropical cyclone (TC), a rapidly rotating storm characterized by a low pressure center originating over tropical oceans, imposes significant damages to human society and natural ecosystem. Hazards from TCs (which include tropical depressions, tropical storms, and hurricanes) include extreme winds, torrential rains triggering floods and/or landslides, and damaging storm surges (Peduzzi et al. 2012). The strong winds and flooding during TCs damage infrastructure including shelter, sanitation, drinking water, electricity supplies, and transportation services, leading to injury and loss of life (Ebi et al. 2021; Pielke et al. 2008; Rappaport 2014), as well as economic losses (Kunze 2021; Wu et al. 2020). Webster et al. (2005) showed that intense TCs have significantly increased across the globe during 1970–2004 with warming of sea surface temperature, especially over North Pacific, Indian, and southwest Pacific Oceans. Destructive tropical cyclones have increased markedly since the mid-1970s, due to their longer lifetime and greater storm intensities (Emanuel 2005). Both theory and modeling predict that the intensity of TCs should increase in the future with warming (Emanuel 1987; Knutson and Tuleya 2004), although there are large uncertainties in projecting the changes in TC frequencies during the twenty-first century (Emanuel et al. 2008; Wu et al. 2014).

TCs could induce extreme hot weathers under certain circumstances. For instance, Typhoon Lekima (2019) contributed greatly to the occurrence of extreme hot days over southeastern coast of China (SECC) by increasing the sensible heat flux through subsidence induced by its outer circulation, favoring extreme heat over there (Zhao et al. 2021). Matthews et al. (2019) underlined the risk of severe heat following significant tropical cyclones, and underscored the severity of the potential effects, since megablackouts may accompany powerful TCs, making it hard to utilize air conditioning during heat days. Such new hazards have impacted around 1000 people along densely populated coastline and may rise markedly in a warming climate (Matthews et al. 2019). On interannual time scale, there are more hot days during active TCs years than less active TCs over southern China (Zhong et al. 2019). SECC is vulnerable to both TCs and HWs in summer season and the compound hazards of TCs and HWs (TC–HWs) could be more destructive to society and natural ecosystem than the individual extremes. However, few works have systematically assessed the impacts of TCs on HWs and evaluated the long-term trends of the compound hazards of TC–HWs over SECC in the warming climate. In this study, we investigate the characteristics and long-term trend of compound TC–heat hazards in SECC during 1960–2019 based on observational datasets for improving understanding of the compound extremes in SECC and other coastal regions of the globe. The work is organized as follows. Data and methods are introduced in section 2. Section 3 presents the main results. Summary and discussion are given in section 4.

2. Methods and data

a. Datasets

We focus on the compound hazards of TC–HWs over SECC (15°–30°N, 105°–125°E) as outlined in Fig. 1. The domain involves most of the TC tracks over western North Pacific (WNP), as shown in Fig. 1b. The TC best track data are released by China Meteorological Administration (CMA) during the historical period of 1960–2019 (accessible at https://tcdata.typhoon.org.cn/zjljsjj_sm.html). The database provides the best track information of TCs over WNP with their names and positions in latitude and longitude (Ying et al. 2014). The datasets have been included in the International Best Track Archive for Climate Stewardship (IBTrACS) project (Knapp et al. 2010), an official World Meteorological Organization (WMO) global resource for TC best track data.

Observed daily maximum surface air temperatures (Tmax) for defining heatwaves are also provided by CMA. The observed datasets have been quality controlled, homogenized, and widely used for studies on the long-term variations of extreme weather events across China (e.g., Liu et al. 2019; Wang et al. 2017). The datasets contain more than 2000 observational sites over China, and 652 of them are included in SECC region (see Fig. S1 in the online supplemental material). The new Japanese 55-year Reanalysis (JRA-55) by the Japan Meteorological Agency (Kobayashi et al. 2015) is also employed to derive the synoptic circulations during TC–HWs, including daily 2 m temperature (T2m), geopotential height, winds, downward solar radiation flux at surface (DSR), vertical velocity (ω), and sensible heat flux at surface (SH). In this study, we focus on the compound hazards during the warm season (May–September), as hot weathers during the warm season (the extended summer period) are more harmful and dangerous, and TC activities over WNP are mainly generated from May to November. Their climatology and anomalies are derived based on the period from 1960 to 2019.

b. Identification of compound extremes of TC–HWs

As in our previous work (Wang et al. 2017), a heatwave is defined as a period of extreme high temperatures that lasts consecutively for at least three days. There is no univocal and optimal way to define a heatwave. The heatwave definitions largely differ in datasets, such as the daily maximum/minimum/average temperatures (Perkins 2015; Wang et al. 2017; Dosio et al. 2018; Hulley et al. 2020), or apparent temperature/heat index as a combination of both humidity and temperatures (P. Wang et al. 2019; Matthews et al. 2019). You et al. (2017) compared the patterns, trends, and variations of heatwaves in China during 1961–2014 among 16 previously published heatwave definitions. It is found that heatwaves in China identified with daily maximum/minimum/average or apparent temperature show consistent geographical patterns and trends. In this work, daily maximum air temperatures in the warm season from May to September are used to define heatwaves and the compound TC–HWs over SECC. We use daily Tmax because of its widespread operational use, not least by the China Meteorological Administration, to issue extreme weather alerts when daily maximum temperatures are at very high levels. The extreme high temperatures occur when the area average of daily Tmax over SECC exceed a local specific threshold. Specifically, for each calendar day during May–September, the threshold is calculated as the

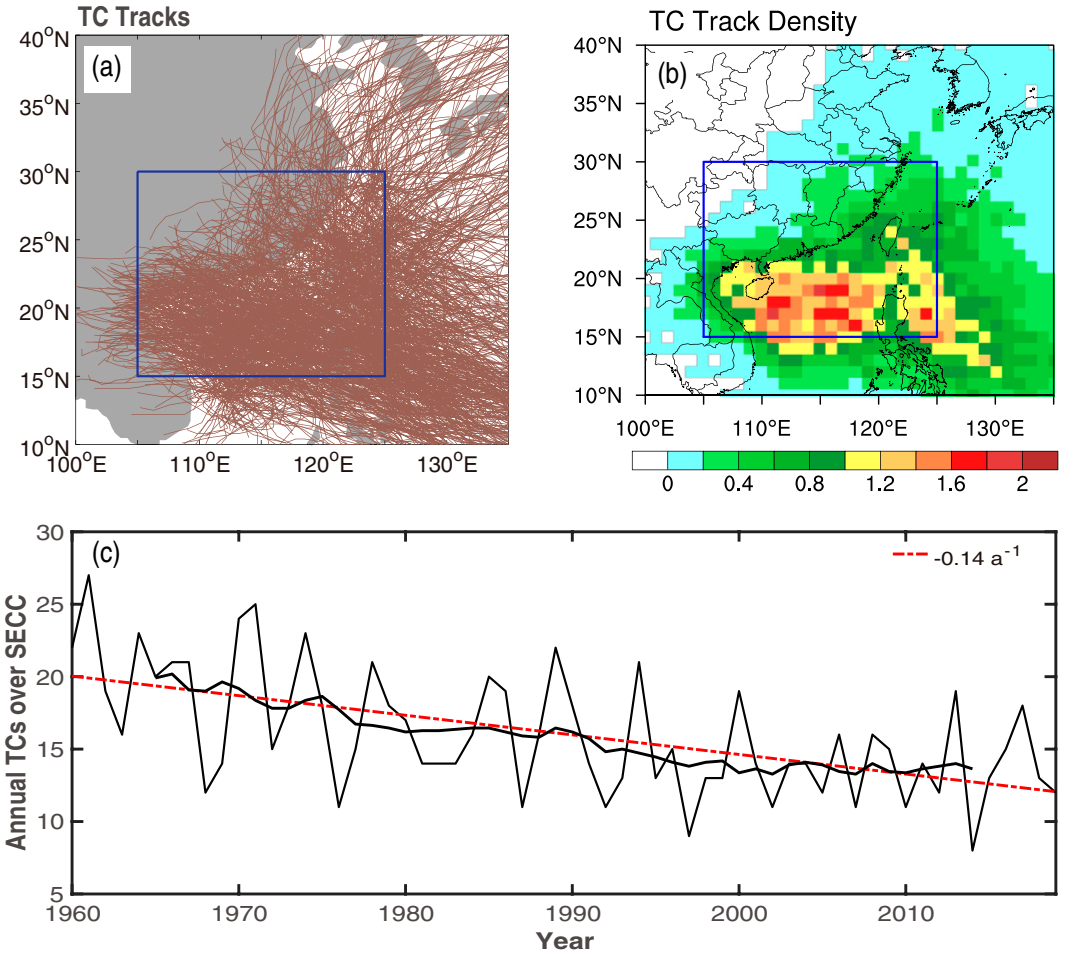

FIG. 1. (a) Tracks of 963 TCs over SECC and (b) TC track densities calculated over 1° × 1° grids for 1960–2019. (c) The annual TCs affecting SECC. The blue rectangle indicates SECC region (15°–30°N, 105°–125°E).

90th percentile of a 21-day moving centered window from 1960 to 2019.

Furthermore, considering the temporal persistence/duration of a TC or HW event, a compound hazard of TC–HW is identified over SECC when a HW occur within the period of 3 days prior to and 3 days following the period when a TC is located over SECC. A compound hazard TC–heat is previously defined in Matthews et al. (2019) when a major TC (central pressure ≤ 945 hPa) followed within 30 days by a heat index (HI) > 40.6°C at the site of landfall. They focused on the extreme cases that a TC first cripples electrical infrastructure and is then followed by deadly heat, which are expected to cause catastrophic consequences. According to their strict criterion, such compound TC–heat events have been vanishingly rare and only four TC–heat events during 1970–2017 were observed around northwest Australia. In particular, it is important to notice in their work that both air temperatures and heat index are anomalously high before TC landfalls, even higher than those days following TC landfalls (their Fig. 3), which inspires us the high probability of the compound events that anomalously high air temperatures over coastal regions occur before TC landfalls. In particular, excluding HWs associated with TC–HWs, HWs that occur alone are referred to as AHWs. By comparing the characteristics of TC–HWs and AHWs and their associated synoptic conditions, we aim to clarify the relationship between TCs and HWs.

Following Wang et al. (2017), HWs as part of both TC–HWs and AHWs are measured from different aspects, including heatwave number (HWN; unit: events), the number of heatwaves that occur in a given time interval, e.g., a year, heatwave amplitude (HWA; °C per event) which indicates the maximum temperature during a heatwave event, heatwave duration (HWDU; unit: days per event) and heatwave frequency (HWF; unit: days) which refers to the total heatwave days during a specific period or a given year.

3. Results

a. Annual variations of TCs and HWs over SECC

TCs that affect the SECC region are identified as those TCs with tracks that intersect the SECC region during their lifetimes.

Accordingly, there are 963 TCs in total that have affected the SECC region during May–September of 1960–2019. Figure 1 presents the TC tracks and TC track densities calculated over 1° × 1° grids in the past 60 years. TCs that affected southern China mainly originate to the east of 125°E and move westward to enter the SECC region, with some making landfall over mainland of eastern China while the others weakening and dissipating over the WNP (Fig. 1a). Two maximum centers of TC track densities can be found east of South China Sea and southeast of Philippines, with more than 1.6 times per year (Fig. 1b). The annual number of TCs affecting SECC exhibit apparent interannual variations with a notable decreasing trend of −1.4 events per decade, significant at the 95% confidence level (Fig. 1c). The decreasing trend of TCs over WNP is consistent with previous works (e.g., Li et al. 2017; Hu et al. 2018; Zhao et al. 2018). For example, Hu et al. (2018) pointed out that the TC genesis frequency in the WNP had been going down steadily and significantly since the 1960s, which is likely contributed by changes in the vertical wind shear and the low-level vorticity, driven by sea surface temperature anomalies (Hu et al. 2018; Zhao et al. 2018).

Figure 2 displays the variations of annual HWN, annual maximum HWA, annual maximum HWDU, and annual HWF for May–September during 1960–2019. The observed annual HWN shows an increasing trend of 0.42 events per decade during 1960–2019 and the increasing trend is stronger since the mid-1980s with a magnitude of 0.91 events per decade (Fig. 2a). Such interdecadal variations are also seen for the annual HWA, HWDU, and HWF, which exhibit an enhanced increasing trend since the mid-1980s, compared to the trends over the longer period (Figs. 2b–d). All the increasing trends of the four indices are significant at 95% confidence level since the mid-1980s. The decadal variations of heatwave frequency over SECC since the 1960s with the lowest values around the mid-1980s have been previously reported (e.g., Wang et al. 2017; You et al. 2017), reflecting the rapid warming since the mid-1980s (as shown in Fig. S2). The mean air temperature over SECC during the warm season exhibits a decreasing trend before the mid-1980s, with the lowest levels occurring between 1970 and 1995, but it has risen significantly since then (Fig. S2). Note that the linear trend of temperatures for the period 1985–2019 is 0.28°C decade^{-1}, significantly higher than the overall linear trend of 0.12°C decade^{-1} for 1960–2019 (Fig. S2), supporting the increasing trends of frequency, duration, and intensity of HWs over SECC. Thus, in the past 60 years, HWs over SECC have been more frequent, stronger and longer lasting due to climate warming. Despite the intensifying HWs in the past decades, TCs that affect SECC have been generally decreasing. Therefore, the potential impacts of TCs on HWs and the long-term trend of their compound extremes (TC–HWs) over SECC deserve further exploration.

b. *Impacts of TCs on HWs over SECC*

Tropical cyclones are hypothesized to affect heat transportation and distribution in the ocean–atmosphere system, making them potentially important modulators of the local and remote weather and climate systems (Mei et al. 2013; Zhong et al. 2019). For example, TCs over WNP have significant impacts on the meridional movements of WPSH (T. Wang et al. 2019), which is one of the major circulation systems that dominate temperature changes and extreme high-temperature events in summer over eastern China (Liu et al. 2019; Deng et al. 2020). Therefore, in the following section, we investigate the potential impacts of TCs on heatwaves over SECC by

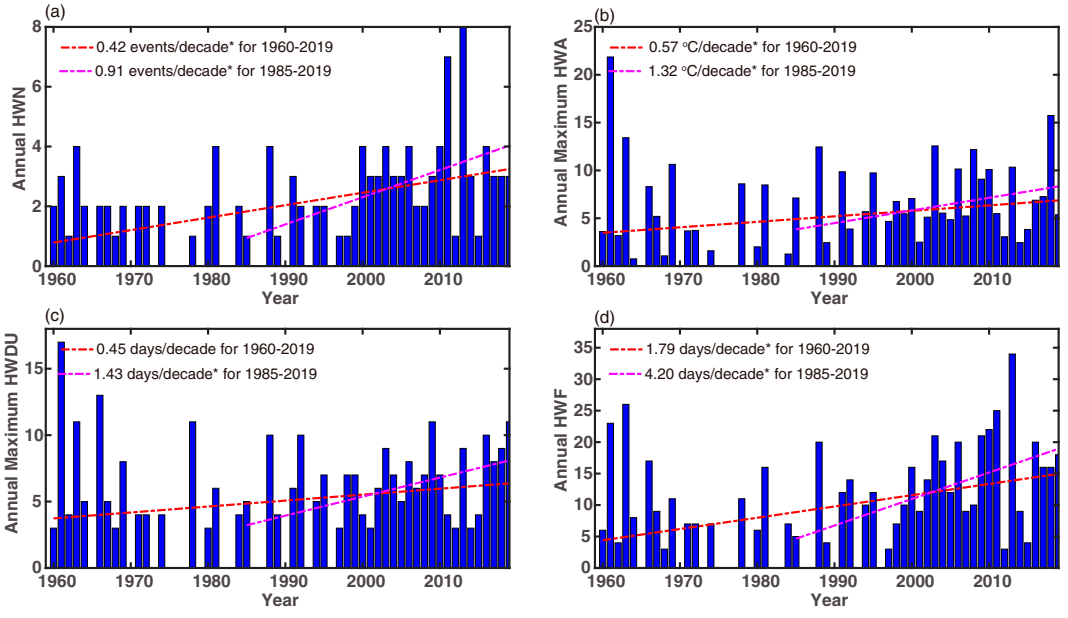

FIG. 2. Time series and linear trends of (a) annual HWN, (b) annual maximum HWA, (c) annual maximum HWDU, and (d) annual HWF over SECC for warm season (May–September) during 1960–2019 (red line) and 1985–2019 (magenta line). Trends marked by asterisk denote significant trends above 95% confidence level.

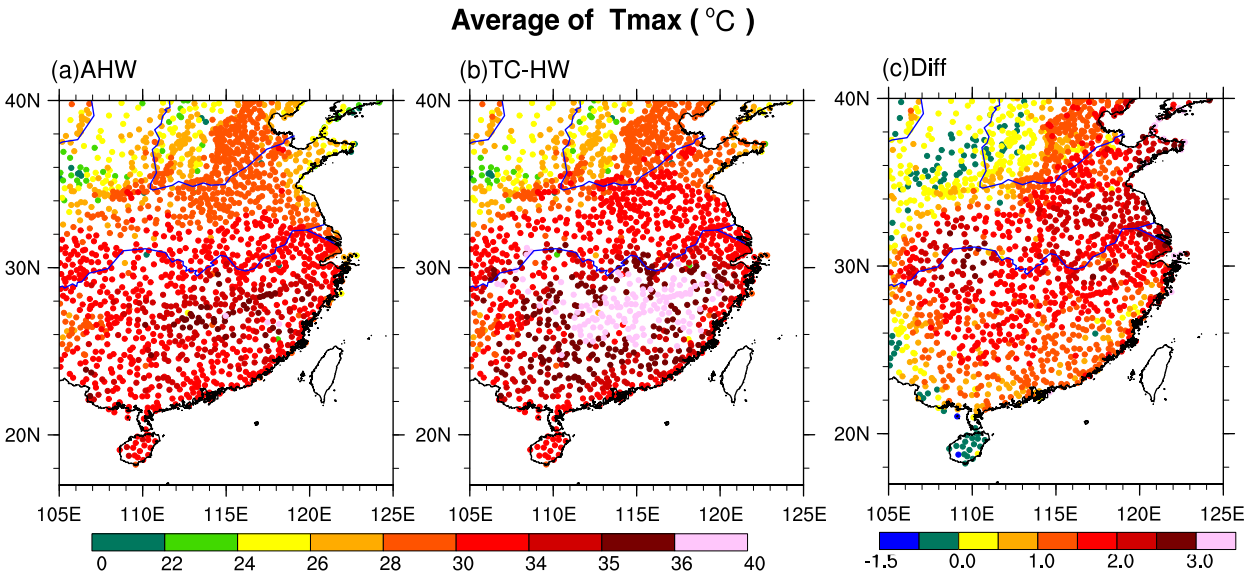

FIG. 3. The spatial pattern of average Tmax during (a) AHWs, (b) TC–HWs, and (c) the differences between AHWs and TC–HWs (the latter minus the former).

disentangling the differences in the synoptic conditions between AHWs and TC–HWs.

Based on the definition of TC–HWs, there are 81 TC–HWs during 1960–2019, accounting for around 70% of the total HWs (121 events), with 40 heatwaves (30%) occurring alone (AHWs) during the past 60 years. Figure 3 presents the spatial distributions of average Tmax during AWHs, TC–HWs and their differences. Higher temperatures centered over SECC are observed during both AHWs (Fig. 3a) and TC–HWs (Fig. 3b), with the maximum above 35°C, the extreme hot level suggested by CMA. Moreover, air temperatures are higher during TC–HWs than AHWs, as hot sites with mean Tmax above 35°C spread nearly across the whole region south of the Yangtze River during TC–HWs while hot temperatures above 35°C are apparent in much fewer locations during AHWs (Figs. 3a,b). The differences of average Tmax between TC–HWs and AHWs further validate that the mean temperatures during TC–HWs are higher than those during AHWs across Southeast China, especially along the Yangtze River basin, with a magnitude above 2.5°C (Fig. 3c). Moreover, the average duration of AHWs and TC–HWs are 4.5 and 5.0 days per event, respectively. Thus, the longer-lasting and stronger compound extreme TC–HWs could cause greater damages to society and ecosystem than heatwaves that occur alone.

Figure 4 shows the composite anomalies of reanalysis 2-m air temperature (T2m) for AHWs, TC–HWs, and their differences. During AHWs, positive T2m anomalies cover a large zonal area over South China with a maximum amplitude exceeding 2.5°C. Note that the approximate locations of seven subregions, including South China, Central China, etc., are labeled on the topography map of China in Fig. S6. For TC–HWs, positive T2m anomalies cover a larger area with the 1.5°C contour extending east to the WNP area, and the SECC region is completely covered by the 2.5°C contour. Thus, consistent with the in situ observation results, TC–HWs feature hotter temperature than AHWs, with T2m differences exceeding 0.5°C over the whole Southeast China and maximum differences above 2°C dominating the Yangtze River basin over land. Note that enhancement in T2m during TC–HWs is also observed over WNP with positive differences in T2m above 3°C.

The spatial patterns of the composite anomalies of surface pressure (PS) and 10-m winds during AHWs, TC–HWs and their differences are presented in Fig. 5. During AHWs, negative PS anomalies cover most of Southeast China while positive PS anomalies dominate WNP with maximum values around the South China Sea region. Meanwhile, anomalous anticyclonic circulations control the low-level atmosphere over tropical WNP with anomalous southwesterly winds influencing SECC (Fig. 5a). In contrast, during TC–HWs, TC-induced negative PS anomalies cover both land and ocean, accompanied by cyclonic circulations over the South China Sea region (Fig. 5b). Thus, the differences of PS and 10-m winds between TC–HWs and AHWs exhibit negative values over the SECC and WNP regions, accompanied by a strong cyclonic circulation over tropical WNP centering around South China sea (Fig. 5c).

The spatial patterns of lower-level to middle-level circulations during AHWs and TC–HWs at 850 and 500 hPa and their differences are further displayed in Figs. 6 and 7. At the 500-hPa level during AHWs, most of the tropical west Pacific Ocean south of 25°N is under the control of the northwestern Pacific subtropical high (WPSH), encircled by the 5860 geopotential meter (gpm) contour line. In addition, significant positive geopotential height (H500) anomalies cover the SECC region and the tropical WNP, with the maximum centered between the Philippines and Hainan Island. Such anomalous pattern indicates the strengthening and southward expansion of WPSH (Fig. 6a). Previous studies have underscored the significant role of WPSH in modulating the occurrence and

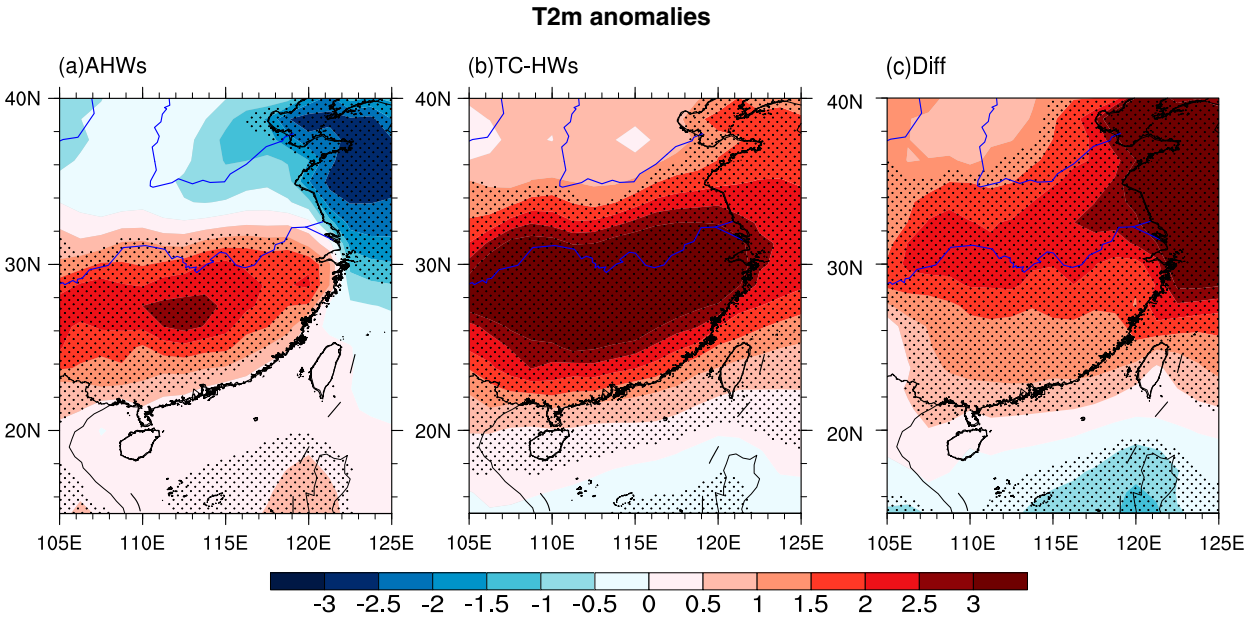

FIG. 4. The spatial pattern of T2m anomalies during (a) AHWs, (b) TC–HWs, and (c) the differences between AHWs and TC–HWs (the latter minus the former). Stippling indicates statistically significant anomalies above 95% confidence level. The anomalies are obtained by removing the climatological mean of May–September.

variations of heatwaves over South China by inducing subsidence that enhances the hot and dry conditions at the surface and thus intensifies heatwaves (Wang et al. 2017). During TC–HWs, positive H500 anomalies cover a large zonal band across Central China, with the maximum centered over central-eastern China while negative H500 anomalies are observed over tropical WNP, in accordance with the surface pressure depression accompanied by TCs (Fig. 6b). In addition, the 5860-gpm contour covers a zonal band of China between 20° and 35°N. Such circulation pattern featured by the anomalous H500 indicates a northward expansion of WPSH (Fig. 6b). Accordingly, the differences of average H500 between AHWs and TC–HWs show negative values over the tropical WNP centered around South China Sea and positive values over China north of 20°N (Fig. 6c). In turn, the anomalous easterlies during TC–HWs along the southern boundary of the enhanced subtropical ridge (Fig. 6c) may strengthen TC activities over tropical WNP (Harry and Elsberry 1991). In brief, compared to AHWs, WPSH during TC–HWs shifts northward because of

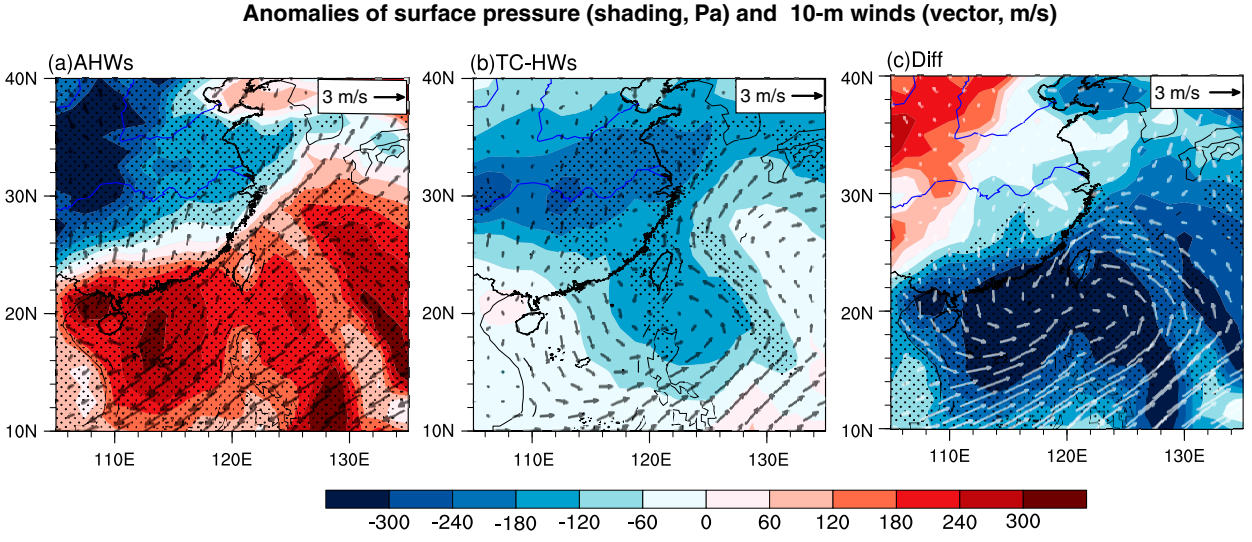

FIG. 5. As in Fig. 4, but for surface pressure (PS; shading) and winds at 10 m (vectors). Stippling indicates statistically significant PS anomalies above 95% confidence level.

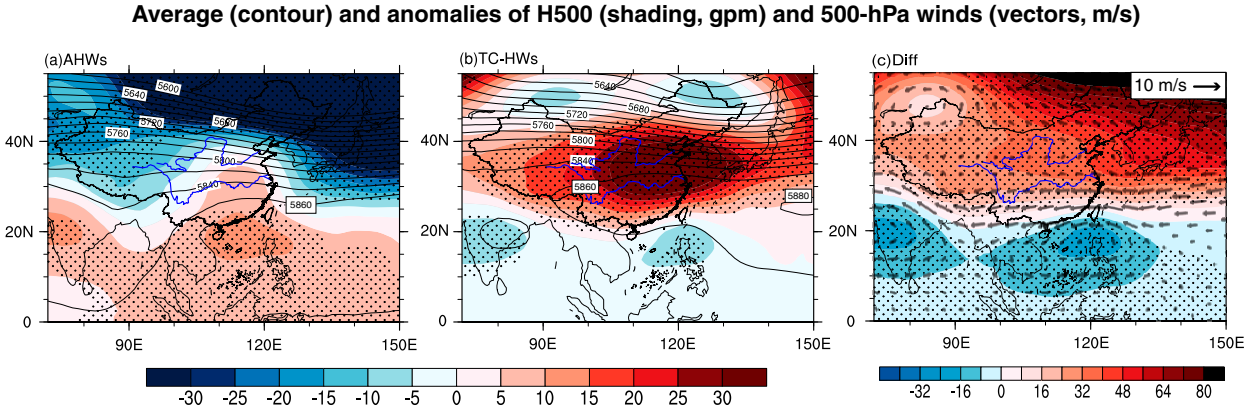

FIG. 6. The spatial pattern of average (contour) and anomalies (shading) of H500 during (a) AHWs and (b) TC–HWs. (c) Differences of the average of H500 (shading) and winds at 500 hPa (vectors) between AHWs and TC–HWs (the latter minus the former). Stippling indicates statistically significant H500 anomalies above 95% confidence level.

TC activities on its southern flank, placing SECC under the dominant influence of WPSH. The associated subsidence and incoming solar radiation associated with WPSH may favor extreme high temperatures.

Atmospheric circulations at 850 hPa exhibit similar patterns to those at 500 hPa. During AHWs, WPSH is also enhanced and expand southward, with the 1480 gpm contour covering areas south of 20°N. Anomalous geopotential height at 850 hPa (H850) during AHWs depicts a dipole pattern with positive anomalies covering the zonal band south of 20°N and negative anomalies over the central to northeastern part of China (Fig. 7a). During TC–HWs, the SECC region is also dominated by the 1480 gpm contour, and H850 anomalies exhibit a tripolar pattern over mainland of China with positive values over SECC and negative values centered in the tropical WNP and the northern part of China (Fig. 7b). And the differences of H850 and 850-hPa winds between AHWs and TC–HWs are similar to those at 500 hPa with negative H850 anomalies and cyclonic circulations over the tropical WNP, centered over South China Sea and positive H850 anomalies north of 20°N across China (Fig. 7c). The enhanced WPSH and accompanying anticyclonic circulation favor the maintenance of more frequent and stronger HWs.

To further clarify the impacts of TC activities on WPSH, the meridional and vertical cross section of wind anomalies over 110°–120°E coinciding with the maximum TC densities (Fig. 1b) during AHWs and TC–HWs and their differences are shown in Fig. 8. Southern China between 10° and 30°N are dominated by strong downward motions from surface to upper troposphere while the northern part of China is influenced by anomalous ascending motions centered around 35°N (Fig. 8a), supporting the increased and reduced T2m over southern and northern China, respectively, in Fig. 4a. During TC–HWs, Central China between 20° and 30°N is dominated by strong descending motions with upper-level convergence, adjoined by anomalous ascending motion north and south of the region (Fig. 8b). The anomalous ascending motion over tropical WNP with upper-level divergence is consistent with the strong TC activities there. Therefore, anomalous ascending motions induced by TC activities over tropical WNP during TC–HWs strongly enhance descending motions over Central China, which intensify the high pressure and cause a northward shift of WPSH. It is well known that

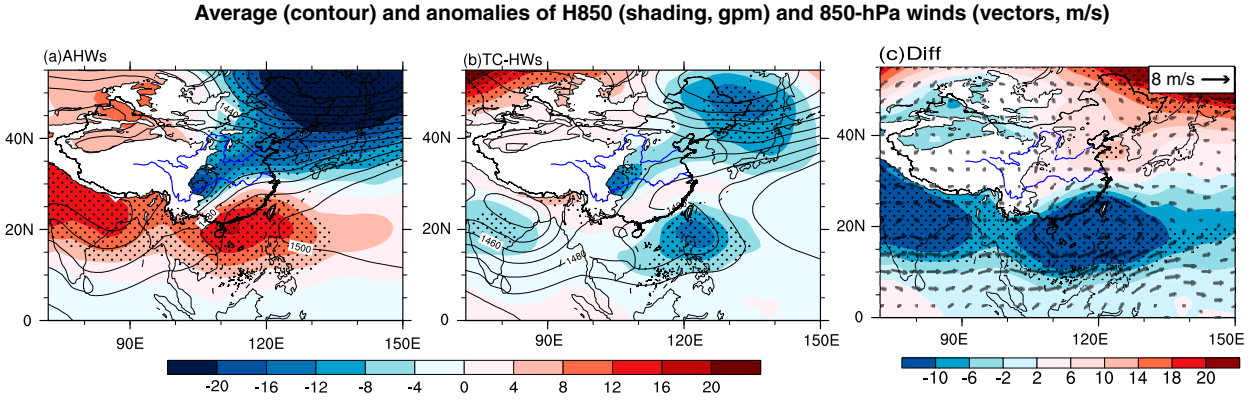

FIG. 7. As in Fig. 6, but for geopotential height and winds at 850 hPa (shading). Areas where the topography is greater than 1500 m (850 hPa in the standard atmosphere) are masked out.

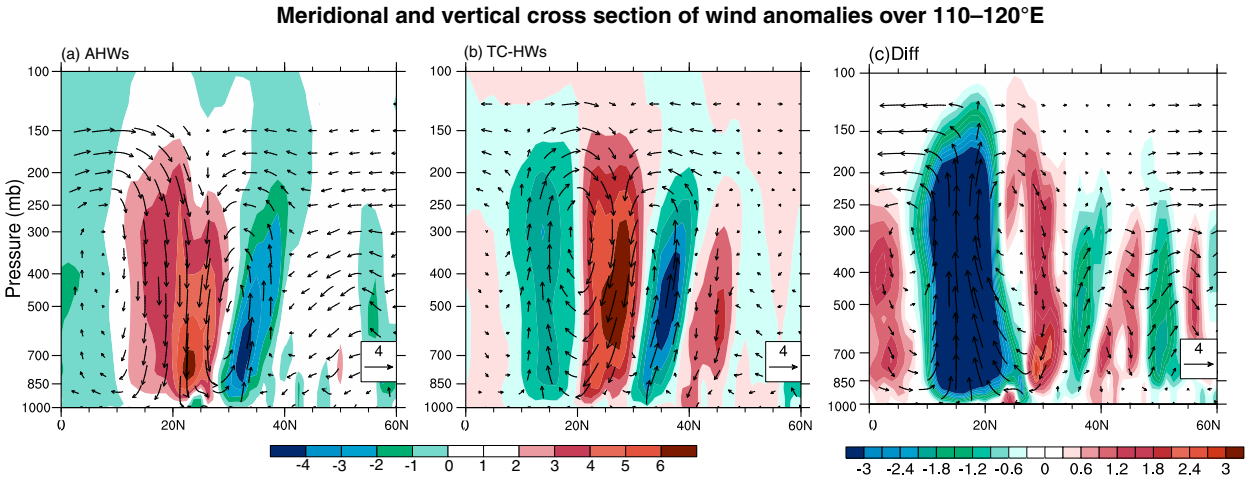

FIG. 8. The meridional and vertical cross section of wind anomalies (vector) over 110°–120°E during (a) AHWs, (b) TC–HWs, and (c) their differences. Shading represents vertical velocity (ω) anomalies (negative values indicate upward motion). Note that ω (Pa s^{-1}) is multiplied by 100 as it is significantly small than zonal winds (m s^{-1}).

anomalous convection over tropical WNP would trigger northward propagation of Rossby waves and cause a meridional displacement of the East Asian monsoon circulation in the summer, as seen in Figs. 6b and 7b, which increases the local temperature through descending motion induced by the high pressure nodes (Nitta 1987; Wang et al. 2017). The difference of vertical circulation between AHWs and TC–HWs highlights the abnormal ascending motion over tropical WNP and descending motion over Central China around 30°N that enhances temperatures through adiabatic heating (Fig. 8c).

Figure 9 further illustrates the spatial patterns of DSR anomalies at the surface during AHWs, TC–HWs and their differences. During both AHWs and TC–HWs, DSR anomalies depict a dipole pattern with increased DSR over southern China and decreased DSR over northern China (Figs. 9a,b). Note that tropical WNP during TC–HWs is controlled by decreased DSR due to the convections associated with TCs while DSR is controlled by increased solar radiations during AHWs, representing clear sky under the control of WPSH (Figs. 9a,b). Thus, Central China during TC–HWs is covered by enhanced DSR relative to AHWs, with a zonal band of positive DSR anomalies dominating between 20° and 30°N across China (Fig. 9c), which partly contribute to the increased temperatures there (seen in Fig. 4c).

Although persistent circulation plays an essential role in triggering heatwaves, their coupling with the land surface is also important. Significant soil moisture deficiency is present in southern China during both AHWs and TC–HWs (Fig. S3). Particularly, soil wetness in southern China is significantly reduced during TC–HWs relative to AHWs while the region to the north is dominated by increased soil moisture (Fig. S3c). Figure S5 demonstrates the composites of daily Tmax and precipitation anomalies before and following the dates when TCs enter SECC. We can

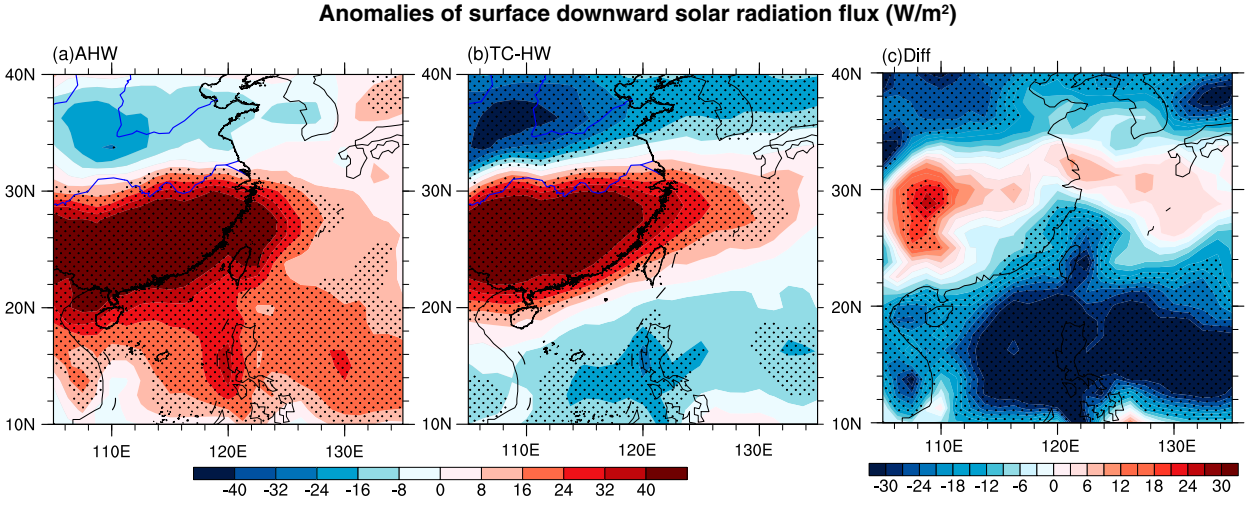

FIG. 9. As in Fig. 5, but for surface downward solar radiation flux (DSR).

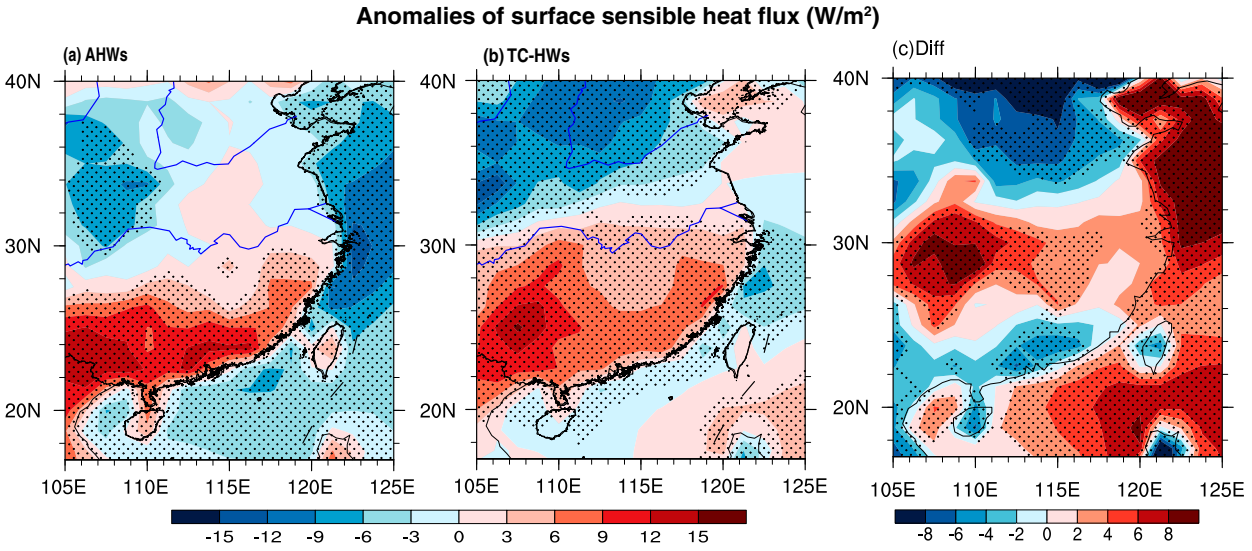

FIG. 10. As in Fig. 5, but for surface sensible heat flux (SH).

see that, following the dates when TCs enter SECC, the observed increases in Tmax over the land region are accompanied by less rainfall, which helps explain the lower soil moisture over land. Note that the precipitation anomalies shift from negative to positive a few days after TC entering SECC, indicating the approaching and landfalls of TC activities. This agrees with the previous finding that rainfall associated with a tropical cyclone can cause dramatic transition from dry soils to exceptional flooding in a very short time from its landfall (Case et al. 2021).

A lack of soil moisture leads to reduced latent cooling and increased SH, which can amplify the surface temperature anomalies (Fischer et al. 2007; Alexander 2011). Consistent with the spatial pattern of soil moisture, SH is significantly enhanced over southern China during both AHWs and TC–HWs (Figs. 10a,b). And the difference in SH between TC–HWs and AHWs demonstrates a positive band between 20° and 30°N across China, with negative values both north and south of the elongated band (Fig. 10c). Note the increased soil moisture and reduced SH over northern China can contribute to the ascending motions over there (Fig. 8c) as wet soils and enhanced evapotranspiration are identified to have positive effects on local convective instability (Seneviratne et al. 2010).

Here, we use a case study of TC Bilis and the heatwave events in July 2006 over SECC to support the proposed relationship between TC and HWs by profiling their day-to-day evolutions. As indicated by its track, Bilis formed over the WNP Ocean and made landfall on the southeastern coast of mainland China on 14 July 2006, persisting over land until 17 July 2006 (Fig. 11a). Following the landfall of TC Bilis, sudden and unforecasted torrential rain commenced some 400 km southwest of the weakening circulation center, and at least 843 people were killed and the direct economic loss was estimated at up to $5 billion (U.S. dollars) in this event (Deng et al. 2017). Though previous works have discussed the impact of Bilis on the heavy rainfall over large areas of southern China (e.g., Gao et al. 2009; Deng et al. 2017; Wang et al. 2009), the potential impacts of Bilis on the hot extremes in that period have been rarely reported. Figures 11b–i illustrate the daily evolution of observational sites with extreme high temperatures exceeding 35°C over the lifetime of Bilis from 9 to 16 July 2006, overlaid by H500 and its anomalies relative to the climatological mean.

On 9 July, two regions of extreme high temperatures were seen over South China, covered/adjoined by positive H500 anomalies. The 5880 gpm contour covers the whole East China Sea with positive H500 centered in northeastern China and extending east to WNP, indicating a northeast extension of WPSH (Fig. 11b). Meanwhile, south of the southern flank of WPSH, negative H500 anomalies centered over Philippine Sea are found, with maximum magnitudes between −45 and −60 gpm. After 9 July, Bilis intensified and the negative H500 anomalies increased gradually and migrated northwestward. Meanwhile, WPSH gradually extended westward, with the 5880 gpm contour covering larger area of China mainland and causing an expansion of the hot sites over southeastern China. Bilis reached its maximum intensity on 12 July with the strongest magnitude and dominance of H500 anomalies over the ocean (and the minimum surface pressure, not shown) (Fig. 11e). On the same day, extreme high temperatures over land peaked with the greatest number of hot sites with the highest Tmax above 43°C. Bilis made landfall on 14 July when it started to recurve (Fig. 11a), and most of the hot sites over southern China experienced a relief because of the cooling effects following the landfall of Bilis. The 5880 gpm contour was consequently split into two parts, of which the northern part that dominated some hot sites over Central China was sustained for a while. Bilis then gradually weakened with decreasing magnitude and dominance of the H500 anomalies and finally dissipated on 17 July (not shown). Therefore, the typical case based on Bilis supports the above mechanisms that TC activities trigger hot extremes over SECC mainly by enhancing the north extension and strengthening of WPSH. Moreover, it is noted that TC activities can enhance hot temperatures before their landfalls and the impacts gradually intensify with their approaching toward land, but

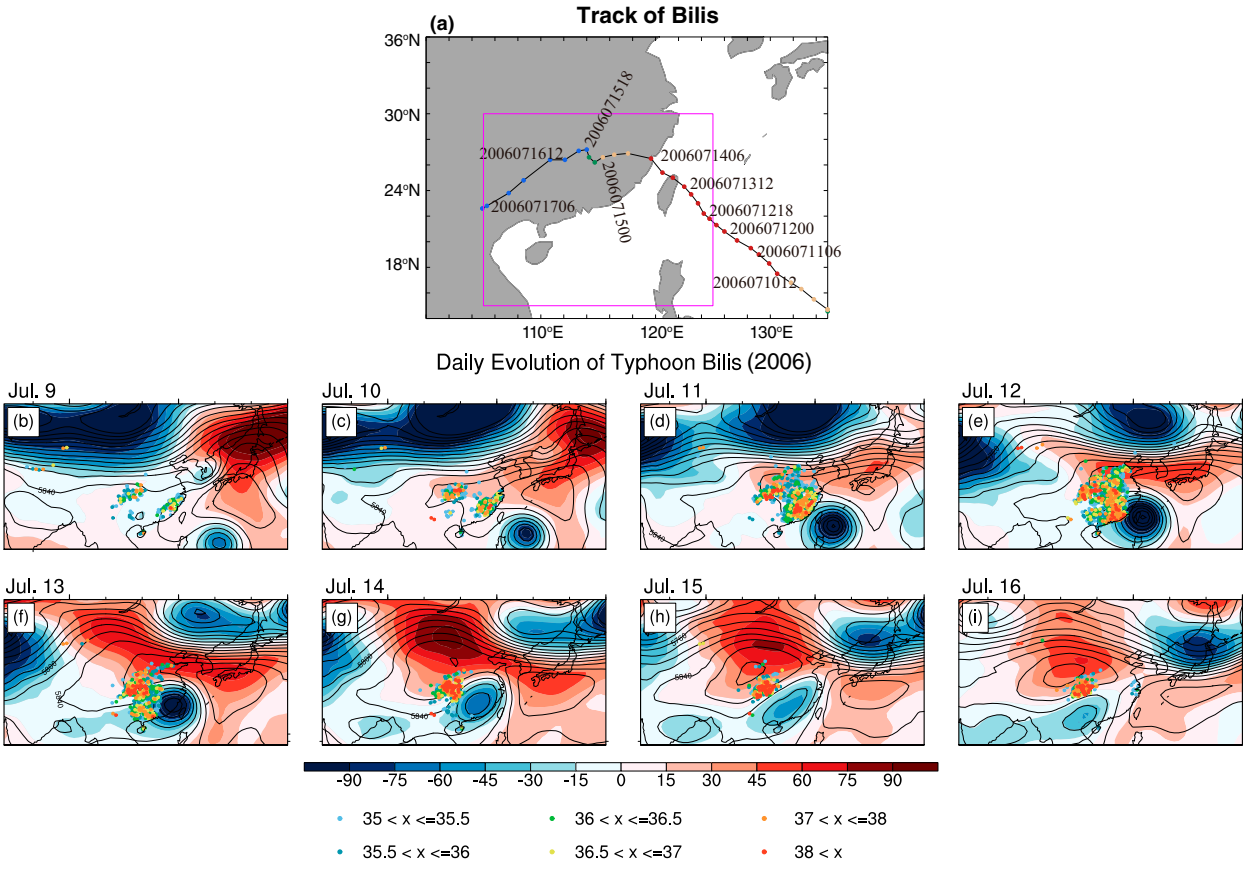

FIG. 11. (a) Track of TC Bilis. (b)–(j) Daily evolution of H500 (contours) and its anomalies (shading) during 8 to 16 Jul 2006. Color dots indicate site with Tmax higher than 35°C.

the enhancement collapses once TCs make landfall because of their cooling effects. It is well known that sinking air is distributed over a wide area on the outer region of TCs. The air subsidence-induced adiabatic warming may also contribute to the local high temperatures over the coastal regions. However, once TCs make their landfalls, cooling effects take place due to the cloudy/rainy days induced by them, which block the solar radiation from reaching the surface.

In fact, the impacts of TCs on the meridional movements of WPSH have been previously evaluated. Based on numerical model simulations, T. Wang et al. (2019) demonstrated that TCs can affect the WPSH meridional movement by stimulating abnormal perturbations that disperse and propagate outwards, prospecting a possible way by which TCs over western North Pacific could affect the weather and climate in East Asia. Note that as Typhoon Bilis gets closer to land, WPSH splits (Figs. 9h,i). This is in line with previous works that TCs turn toward the northeast over the western Pacific Ocean would cause WPSH to split (e.g., Zhong 2006).

c. *Long-term trend of TC–HWs over SECC*

The above analyses support the substantial enhancements of TCs over tropical WNP on HWs over SECC. Accordingly, there is a significant concurrent relationship between TCs over WNP and HWs over SECC. There are 81 events of TC–HWs and 40 events of AHWs during 1960–2019. Thus, most of HWs over SECC (around 70%) are accompanied by TCs over tropical WNP. Figure 12 shows that both AHWs and TC–HWs exhibit interannual and interdecadal variations with increasing trends since the mid-1980s, consistent with the changes in total HWs (Fig. 2a). Even though the total number of TCs passing through the SECC region has decreased since 1960s (Fig. 1c), the fraction of TCs associated with TC–HWs has increased significantly since the mid-1980s. It is worth noting that, in the past decades, there have been no significant increases in the intensity of TCs over SECC (Fig. S4). Therefore, the increasing co-occurrences of TCs and HWs over SECC are mainly driven by the increasing frequency of HWs during 1960–2019 (Fig. 2). It could be concluded that the warming climate favors the rising TC–HWs over SECC due to the increasing HWs. HWs in China are expected to be more frequent and intense under the continued warming climate, while TC frequency over WNP is likely to decrease, suggesting the uncertainties in the future changes in the compound HW–TCs.

In the long-term perspective, climate warming substantially influences the relationship between TCs and hot temperatures over SECC. Figure 13 demonstrates the observed Tmax anomalies

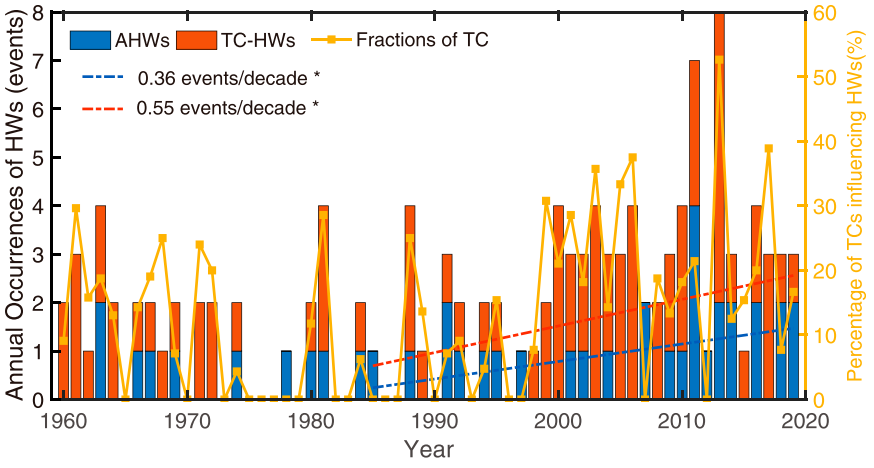

FIG. 12. Annual occurrences of AHWs and TC–HWs (bar), and the percentages of TCs (yellow line) associated with TC–HWs relative to total TCs during 1960–2019. Blue and red dashed lines denote the linear trends of AHWs and TC–HWs during 1985–2019. Trends marked by asterisk denote significant trends above 95% confidence level.

averaged for the SECC region from 20 days ahead to 20 days following the period when TCs are located in the SECC during 1960–2019. Positive Tmax anomalies are mainly found to the right of the zero point on the x axis after TCs entered the SECC region, indicating the anomalous warm temperatures over land are triggered by the approaching TCs. Notably, the Tmax anomalies gradually decrease and eventually become negative in a few days, signifying landfalling of the TCs. This long-term analysis supports the case study of Bilis that TCs enhance hot temperatures before their landfalls while the enhancement collapses once they make landfalls. Moreover, consistent with the increasing air temperatures in the past decades, especially since the mid-1980s (Fig. S2), the Tmax anomalies associated with TC activities have been obviously enhanced since then. The increasing trend of temperature anomalies over SECC should be linked to the warming trend in China during the past decades, which has been previously recognized based on station observations (e.g., Zhao et al. 2014; Cao et al. 2016). Using the reconstructed continuous and homogenized surface air temperature (SAT) series for 16 cities across eastern China, Zhao et al. (2014) found a significant increasing trend of SAT since 1951. It was also found that anomalies of large-scale climate indices such as the tropical Indian Ocean sea surface temperatures (SSTs) and the Siberian atmospheric circulation systems accounted for at least 80% of the total warming trends. The mechanisms linking the oceanic oscillations and regional climate changes remain an interesting topic for further studies. In addition, the effect of urbanization and land-use changes should have also played a role in the observed warming in China (Jones et al. 2008; Sun et al. 2016).

Moreover, as illustrated in Fig. S5, the peak of averaged positive temperature anomalies during 1960–2019 coincides with the peak of rainfall deficiency, suggesting the dominance of

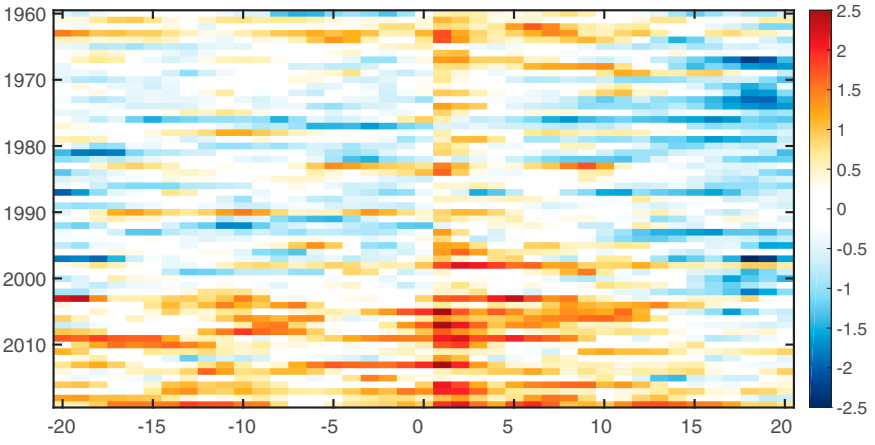

FIG. 13. Observed Tmax anomalies (°C) averaged for the SECC region from 20 days ahead of to 20 days following the dates when TCs enter the SECC region during 1960–2019. Anomalies are calculated from a day-of-year climatology.

strong air subsidence with reduced rainfall. Therefore, the temperature increases following the dates when TCs enter SECC should be mainly contributed by the subsidence associated with WPSH and/or the TC outer region. Note that the positive temperature anomalies weaken gradually after reaching the peak and persist for approximately 10 days with slightly positive rainfall anomalies until a heavy rainfall interrupts. The weakened temperature increases following it peak value are likely partly contributed by the warm core accompanied by a slight rainfall. Still, further assessments with reliable observational data or model simulations of the vertical structures of TCs that affect HWs over SECC are needed to figure out the details.

4. Discussion and conclusions

Currently, concerns about the impacts of TCs have mainly focused on the associated extensive floods, landslides, and storm surge. With observational and reanalysis datasets during 1960–2019, this present study shows a remarkable concurrent relationship between extreme heatwaves and TC activities over SECC. HWs over SECC are mostly accompanied by TC over tropical WNP (TC–HWs) and these are stronger and longer lasting than those occurring alone (AHWs), with average Tmax differences up to 2.5°C in observations. The enhancement on HWs caused by TCs gradually intensifies until TCs make landfalls and then collapses. In the long term, although the total frequency of TCs over WNP that affect the SECC region gradually decreased during 1960–2019, their co-occurrences with extreme heatwaves are increasing. In this work, we attribute the increases in TC–HWs primarily to the rising HWs in the past few decades, as the frequency of TCs over the WNP has been gradually declining during 1960–2019. However, the mechanisms can be intricate and comprise multiple possibilities. As shown in Fig. S7, excluding the effects of global warming on air temperature does not eliminate the impacts of TCs on high temperatures. When a TC approaches the SECC land region, the average Tmax rises therein (Fig. S7b). Moreover, the enhancements of TCs on air temperatures have become notably more pronounced in recent decades, particularly since the 2000s (Fig. S7a). This indicates that TCs over WNP in recent decades may be more likely to induce HW over SECC region. In addition, as mentioned above, the proportions of TCs that are accompanied by HWs have increased in recent decades, particularly since the mid-1980s while the frequency of TCs has been gradually declining. Consequently, this raises the possibility that the more frequent and stronger HWs in recent decades favor more TCs affecting the SECC region. To figure out the interactions between TCs and HWs, more research with model simulations is necessary.

Based on composite analysis during TC–HWs, AHWs and their comparisons, it is found that TC activities over tropical WNP affect summer circulations over eastern China mainland. Compared to atmospheric conditions during AHWs, surface air temperatures are apparently enhanced during TC–HWs. It has been widely known that diabatic heating associated with anomalous convective activities over tropical western Pacific triggers Rossby wave trains propagating northward along East Asia, which favor more hot extremes through descending motion over the high pressure nodes (Wang et al. 2017). Triggered by the strong convections associated with TC activities, large-scale circulations present anomalous meridional patterns with increased geopotential heights over Central China accompanied by strong descending motion from upper troposphere to near surface, which reinforces WPSH and surface solar radiation. Thus, compared to AHWs, TC activities over tropical WNP during TC–HWs enhance HWs by modulating atmospheric circulations and triggering anomalous descending motion over southern China mainland, which intensifies the WPSH and favors increased temperatures. Besides the intensification in WPSH, land–atmosphere coupling also plays a role in modulating HWs. Particularly, descending motion suppresses rainfall over southern China, which favors drier land surface and enhances SH that contributes to higher temperatures over Central China during TC–HWs. The substantial enhancements of TC activities over WNP on HWs over coastal mainland China, as highlighted in this work, warrants further in-depth assessments, such as whether the intensity of TCs can influence their effects on HWs. Moreover, it is worth noting that the interannual variability of WPSH and TC activities over WNP is significantly regulated by the interannual fluctuations of El Niño–Southern Oscillation (ENSO). During La Niña years, the anomalously warmer SSTs over the western Pacific warm pool enhance the warm convections, favoring more TC activities over WNP and leading to the northward shift of WPSH (e.g., Xue et al. 2017). In contrast, WPSH tends to retreat eastward with weakened intensity in El Niño developing summer, while an opposite anomaly is found in the decaying summer (Fu and Teng 1988). Recent studies pointed out the increased ENSO SST variability under the warming climate (Cai et al. 2014, 2022), motivating more works to understand how ENSO could affect the compound TC–HWs under climate warming.

As discussed above, stronger HWs over SECC are exacerbated by TC passages, likely having a greater impact on the coastal populations. Furthermore, before people can recover from heatwaves, heavy rainfall associated with TC activities is another danger. This suggests that the compound hazards of TC–HWs could pose greater risks than the individual extremes alone. For instance, TC Bilis (the fourth strongest tropical storm in 2006) hit southwest China on 14 July (see Fig. 11), and killed more than 800 people. Before the landfall of Bilis, most of southern and Central China had been experiencing a strong heatwave for a while, with daily maximum temperature reaching 38°C, posing a serious threat to human life. Although there are uncertainties in the future frequency of the compound extremes of TC–HWs, their occurrences are likely more dangerous in the near future, as TC intensity and destructiveness are projected to increase (Peduzzi et al. 2012), along with stronger and more frequent HWs (Wang et al. 2018b) under the climate warming. The potential of stronger TC–HW occurrences necessitates more efforts for planning and adapting to the multiple risks of TC–HWs under climate warming.

Acknowledgments. This work was supported by the National Natural Science Foundation of China (Grants 42105166 and 42105051) and the Science and Technology Project of

Beijing Meteorological Service (BMBKJ202003009). L. Ruby Leung was supported by the U.S. Department of Energy Office of Science Biological and Environmental Research through the Regional and Global Model Analysis program area. The Pacific Northwest National Laboratory (PNNL) is operated for the Department of Energy by Battelle Memorial Institute under Contract DE-AC05-76RL01830.

Data availability statement. Daily maximum air temperature is provided by the National Meteorological Information Centre of the China Meteorological Administration (http://data.cma.cn/en/). Reanalysis datasets are derived from the new Japanese 55-year Reanalysis (https://doi.org/10.5065/D6HH6H41, https://rda.ucar.edu/datasets/ds628.0/, Japan Meteorological Agency/Japan, 2013).

REFERENCES

Alexander, L., 2011: Extreme heat rooted in dry soils. *Nat. Geosci.*, **4**, 12–13, https://doi.org/10.1038/ngeo1045.

Barriopedro, D., E. M. Fischer, J. Luterbacher, R. M. Trigo, and R. García-Herrera, 2011: The hot summer of 2010: Redrawing the temperature record map of Europe. *Science*, **332**, 220–224, https://doi.org/10.1126/science.1201224.

Borden, K. A., and S. L. Cutter, 2008: Spatial patterns of natural hazards mortality in the United States. *Int. J. Health Geogr.*, **7**, 64, https://doi.org/10.1186/1476-072X-7-64.

Budd, G. M., 2008: Wet-bulb globe temperature (WBGT)—Its history and its limitations. *J. Sci. Med. Sport*, **11**, 20–32, https://doi.org/10.1016/j.jsams.2007.07.003.

Cai, W., and Coauthors, 2014: Increasing frequency of extreme El Niño events due to greenhouse warming. *Nat. Climate Change*, **4**, 111–116, https://doi.org/10.1038/nclimate2100.

——, B. Ng, G. Wang, A. Santoso, L. Wu, and K. Yang, 2022: Increased ENSO sea surface temperature variability under four IPCC emission scenarios. *Nat. Climate Change*, **12**, 228–231, https://doi.org/10.1038/s41558-022-01282-z.

Cao, L., Y. Zhu, G. Tang, F. Yuan, and Z. Yan, 2016: Climatic warming in China according to a homogenized data set from 2419 stations. *Int. J. Climatol.*, **36**, 4384–4392, https://doi.org/10.1002/joc.4639.

Case, J. L., L. T. Wood, J. L. Blaes, K. D. White, C. R. Hain, and C. J. Schultz, 2021: Soil moisture responses associated with significant tropical cyclone rainfall events. *J. Oper. Meteor.*, **9**, 1–17, https://doi.org/10.15191/nwajom.2021.0901.

Deng, D., N. E. Davidson, L. Hu, K. J. Tory, M. C. N. Hankinson, and S. Gao, 2017: Potential vorticity perspective of vortex structure changes of Tropical Cyclone Bilis (2006) during a heavy rain event following landfall. *Mon. Wea. Rev.*, **145**, 1875–1895, https://doi.org/10.1175/MWR-D-16-0276.1.

Deng, K., S. Yang, D. Gu, A. Lin, and C. Li, 2020: Record-breaking heat wave in southern China and delayed onset of South China Sea summer monsoon driven by the Pacific subtropical high. *Climate Dyn.*, **54**, 3751–3764, https://doi.org/10.1007/s00382-020-05203-8.

Dosio, A., L. Mentaschi, M. F. Fischer, and K. Wyser, 2018: Extreme heat waves under 1.5°C and 2°C global warming. *Environ. Res. Lett.*, **13**, 054006, https://doi.org/10.1088/1748-9326/aab827.

Ebi, K. L., and Coauthors, 2021: Extreme weather and climate change: Population health and health system implications. *Annu. Rev. Public Health*, **42**, 293–315, https://doi.org/10.1146/annurev-publhealth-012420-105026.

Emanuel, K. A., 1987: The dependence of hurricane intensity on climate. *Nature*, **326**, 483–485, https://doi.org/10.1038/326483a0.

——, 2005: Increasing destructiveness of tropical cyclones over the past 30 years. *Nature*, **436**, 686–688, https://doi.org/10.1038/nature03906.

——, R. Sundararajan, and J. Williams, 2008: Hurricanes and global warming: Results from downscaling IPCC AR4 simulations. *Bull. Amer. Meteor. Soc.*, **89**, 347–368, https://doi.org/10.1175/BAMS-89-3-347.

Feudale, L., and J. Shukla, 2011: Influence of sea surface temperature on the European heat wave of 2003 summer. Part I: An observational study. *Climate Dyn.*, **36**, 1691–1703, https://doi.org/10.1007/s00382-010-0788-0.

Fischer, E. M., S. I. Seneviratne, P. L. Vidale, D. Lüthi, and C. Schär, 2007: Soil moisture–atmosphere interactions during the 2003 European summer heat wave. *J. Climate*, **20**, 5081–5099, https://doi.org/10.1175/JCLI4288.1.

Fu, C., and X. Teng, 1988: Climate anomalies in China associated with E1 Niño/Southern Oscillation. *Sci. Atmos. Sin.*, **12**, 133–141, https://doi.org/10.3878/j.issn.1006-9895.1988.t1.11.

Gao, S., Z. Meng, F. Zhang, and L. F. Bosart, 2009: Observational analysis of heavy rainfall mechanisms associated with severe Tropical Storm Bilis (2006) after its landfall. *Mon. Wea. Rev.*, **137**, 1881–1897, https://doi.org/10.1175/2008MWR2669.1.

Harr, P. A., and R. L. Elsberry, 1991: Tropical cyclone track characteristics as a function of large-scale circulation anomalies. *Mon. Wea. Rev.*, **119**, 1448–1468, https://doi.org/10.1175/1520-0493(1991)119<1448:TCTCAA>2.0.CO;2.

Hu, F., T. Li, J. Liu, M. Bi, and M. Peng, 2018: Decrease of tropical cyclone genesis frequency in the western North Pacific since 1960s. *Dyn. Atmos. Oceans*, **81**, 42–50, https://doi.org/10.1016/j.dynatmoce.2017.11.003.

Hulley, G. C., B. Dousset and B. H. Kahn, 2020: Rising trends in heatwave metrics across Southern California. *Earth's Future*, **8**, e2020EF001480, https://doi.org/10.1029/2020EF001480.

IPCC, 2021: *Climate Change 2021: The Physical Science Basis*. V. Masson-Delmotte et al., Eds., Cambridge University Press, 2391 pp.

Jones, P. D., D. H. Lister, and Q. Li, 2008: Urbanization effects in large-scale temperature records, with an emphasis on China. *J. Geophys. Res.*, **113**, D16122, https://doi.org/10.1029/2008JD009916.

Knapp, K. R., M. C. Kruk, D. H. Levinson, H. J. Diamond, and C. J. Neumann, 2010: The International Best Track Archive for Climate Stewardship (IBTrACS) unifying tropical cyclone data. *Bull. Amer. Meteor. Soc.*, **91**, 363–376, https://doi.org/10.1175/2009BAMS2755.1.

Knutson, T. R., and R. E. Tuleya, 2004: Impact of CO_2-induced warming on simulated hurricane intensity and precipitation: Sensitivity to the choice of climate model and convective parameterization. *J. Climate*, **17**, 3477–3495, https://doi.org/10.1175/1520-0442(2004)017<3477:IOCWOS>2.0.CO;2.

Kobayashi, S., and Coauthors, 2015: The JRA-55 reanalysis: General specifications and basic characteristics. *J. Meteor. Soc. Japan*, **93**, 5–48, https://doi.org/10.2151/jmsj.2015-001.

Kovats, R. S., and S. Hajat, 2008: Heat stress and public health: A critical review. *Annu. Rev. Public Health*, **29**, 41–55, https://doi.org/10.1146/annurev.publhealth.29.020907.090843.

Kunze, S., 2021: Unraveling the effects of tropical cyclones on economic sectors worldwide: Direct and indirect impacts. *Environ. Resour. Econ.*, **78**, 545–569, https://doi.org/10.1007/s10640-021-00541-5.

Li, R. C. Y., W. Zhou, C. M. Shun, and T. C. Lee, 2017: Change in destructiveness of landfalling tropical cyclones over China in recent decades. *J. Climate*, **30**, 3367–3379, https://doi.org/10.1175/JCLI-D-16-0258.1.

Liu, Q., T. Zhou, H. Mao, and C. Fu, 2019: Decadal variations in the relationship between the western Pacific subtropical high and summer heat waves in East China. *J. Climate*, **32**, 1627–1640, https://doi.org/10.1175/JCLI-D-18-0093.1.

Matthews, T., R. L. Wilby, and C. Murphy, 2019: An emerging tropical cyclone–deadly heat compound hazard. *Nat. Climate Change*, **9**, 602–606, https://doi.org/10.1038/s41558-019-0525-6.

Mei, W., F. Primeau, J. C. McWilliams, and C. Pasquero, 2013: Sea surface height evidence for long-term warming effects of tropical cyclones on the ocean. *Proc. Natl. Acad. Sci. USA*, **110**, 15 207–15 210, https://doi.org/10.1073/pnas.1306753110.

Nitta, T., 1987: Convective activities in the tropical western Pacific and their impact on the Northern Hemisphere summer circulation. *J. Meteor. Soc. Japan*, **65**, 373–390, https://doi.org/10.2151/jmsj1965.65.3_373.

Peduzzi, P., B. Chatenoux, H. Dao, A. De Bono, C. Herold, J. Kossin, F. Mouton, and O. Nordbeck, 2012: Global trends in tropical cyclone risk. *Nat. Climate Change*, **2**, 289–294, https://doi.org/10.1038/nclimate1410.

Perkins, S. E., 2015: A review on the scientific understanding of heatwaves—Their measurement, driving mechanisms, and changes at the global scale. *Atmos. Res.*, **164–165**, 242–267, https://doi.org/10.1016/j.atmosres.2015.05.014.

Pielke, R. A., Jr., J. Gratz, C. W. Landsea, D. Collins, M. A. Saunders, and R. Musulin, 2008: Normalized hurricane damage in the United States: 1900–2005. *Nat. Hazards Rev.*, **9**, 29–42, https://doi.org/10.1061/(ASCE)1527-6988(2008)9:1(29).

Rappaport, E. N., 2014: Fatalities in the United States from Atlantic tropical cyclones: New data and interpretation. *Bull. Amer. Meteor. Soc.*, **95**, 341–346, https://doi.org/10.1175/BAMS-D-12-00074.1.

Rohini, P., M. Rajeevan, and A. K. Srivastava, 2016: On the variability and increasing trends of heat waves over India. *Sci. Rep.*, **2**, 26153, https://doi.org/10.1038/srep26153.

Seneviratne, S. I., T. Corti, E. L. Davin, M. Hirschi, E. B. Jaeger, I. Lehner, B. Orlowsky, and A. J. Teuling, 2010: Investigating soil moisture–climate interactions in a changing climate: A review. *Earth-Sci. Rev.*, **99**, 125–161, https://doi.org/10.1016/j.earscirev.2010.02.004.

Sherwood, S. C., and M. Huber, 2010: An adaptability limit to climate change due to heat stress. *Proc. Natl. Acad. Sci. USA*, **107**, 9552–9555, https://doi.org/10.1073/pnas.0913352107.

Sun, Y., X. Zhang, G. Ren, F. W. Zwiers, and T. Hu, 2016: Contribution of urbanization to warming in China. *Nat. Climate Change*, **6**, 706–709, https://doi.org/10.1038/nclimate2956.

Wang, D., X. Li, W.-K. Tao, Y. Liu, and H. Zhou, 2009: Torrential rainfall processes associated with a landfall of severe Tropical Storm Bilis (2006): A two-dimensional cloud-resolving modeling study. *Atmos. Res.*, **91**, 94–104, https://doi.org/10.1016/j.atmosres.2008.07.005.

Wang, P., J. Tang, X. Sun, S. Wang, J. Wu, X. Dong, and J. Fang, 2017: Heatwaves in China: Definitions, leading patterns and connections to large-scale atmospheric circulation and SSTs. *J. Geophys. Res. Atmos.*, **122**, 10 679–10 699, https://doi.org/10.1002/2017JD027180.

——, ——, S. Wang, X. Dong, and J. Fang, 2018a: Regional heatwaves in China: A cluster analysis. *Climate Dyn.*, **50**, 1901–1917, https://doi.org/10.1007/s00382-017-3728-4.

——, P. Hui, D. Xue, and J. Tang, 2018b: Future projection of heat waves over China under global warming within the CORDEX-EA-II project. *Climate Dyn.*, **53**, 957–973, https://doi.org/10.1007/s00382-019-04621-7.

——, L. R. Leung, J. Lu, F. Song, and J. Tang, 2019: Extreme wet-bulb temperatures in China: The significant role of moisture. *J. Geophys. Res. Atmos.*, **124**, 11 944–11 960, https://doi.org/10.1029/2019JD031477.

——, Y. Yang, J. Tang, L. R. Leung, and H. Liao, 2021: Intensified humid heat events under global warming. *Geophys. Res. Lett.*, **48**, e2020GL091462, https://doi.org/10.1029/2020GL091462.

Wang, T., Z. Zhong, Y. Sun, and J. Wang, 2019: Impacts of tropical cyclones on the meridional movement of the western Pacific subtropical high. *Atmos. Sci. Lett.*, **20**, e893, https://doi.org/10.1002/asl.893.

Wang, W., W. Zhou, X. Li, X. Wang, and D. Wang, 2016: Synoptic-scale characteristics and atmospheric controls of summer heat waves in China. *Climate Dyn.*, **46**, 2923–2941, https://doi.org/10.1007/s00382-015-2741-8.

Webster, P. J., G. J. Holland, J. A. Curry, and H.-R. J. S. Chang, 2005: Changes in tropical cyclone number, duration, and intensity in a warming environment. *Science*, **309**, 1844–1846, https://doi.org/10.1126/science.1116448.

Wu, L., and Coauthors, 2014: Simulations of the present and late-twenty-first-century western North Pacific tropical cyclone activity using a regional model. *J. Climate*, **27**, 3405–3424, https://doi.org/10.1175/JCLI-D-12-00830.1.

——, Z. Wen, and R. Huang, 2020: Tropical cyclones in a warming climate. *Sci. China Earth Sci.*, **63**, 456–458, https://doi.org/10.1007/s11430-019-9574-4.

Wu, Z., H. Lin, J. Li, Z. Jiang, and T. Ma, 2012: Heat wave frequency variability over North America: Two distinct leading modes. *J. Geophys. Res.*, **117**, D02102, https://doi.org/10.1029/2011JD016908.

WWA, 2021: Western North American extreme heat virtually impossible without human-caused climate change. World Weather Attribution, https://www.worldweatherattribution.org/western-north-american-extreme-heat-virtually-impossible-without-human-caused-climate-change/#:~:text=In%20summary%2C%20an%20event%20such,become%20a%20lot%20less%20rare.

Xue, F., X. Dong, and R.-P. Lin, 2017: Two anomalous convective systems in the tropical western Pacific and their influences on the East Asian summer monsoon. *Atmos. Ocean. Sci. Lett.*, **10**, 319–324, https://doi.org/10.1080/16742834.2017.1328969.

Yao, R., Y. Hu, P. Sun, Y. Bian, R. Liu, and S. Zhang, 2022: Effects of urbanization on heat waves based on the wet-bulb temperature in the Yangtze River delta urban agglomeration, China. *Urban Climate*, **41**, 101067, https://doi.org/10.1016/j.uclim.2021.101067.

Ying, M., W. Zhang, H. Yu, X. Lu, J. Feng, Y. Fan, Y. Zhu, and D. Chen, 2014: An overview of the China Meteorological Administration tropical cyclone database. *J. Atmos. Oceanic Technol.*, **31**, 287–301, https://doi.org/10.1175/JTECH-D-12-00119.1.

You, Q., Z. Jiang, L. Kong, Z. Wu, Y. Bao, S. Kang, and N. Pepin, 2017: A comparison of heat wave climatologies and trends in China based on multiple definitions. *Climate Dyn.*, **48**, 3975–3989, https://doi.org/10.1007/s00382-016-3315-0.

Zhao, D., Y. Lin, Y. Li, and X. Gao, 2021: An extreme heat event induced by Typhoon Lekima (2019) and its contributing

factors. *J. Geophys. Res. Atmos.*, **126**, e2021JD034760, https://doi.org/10.1029/2021JD034760.

Zhao, J., R. Zhan, Y. Wang, and H. Xu, 2018: Contribution of the interdecadal Pacific oscillation to the recent abrupt decrease in tropical cyclone genesis frequency over the western North Pacific since 1998. *J. Climate*, **31**, 8211–8224, https://doi.org/10.1175/JCLI-D-18-0202.1.

Zhao, P., P. Jones, L. Cao, Z. Yan, S. Zha, Y. Zhu, Y. Yu, and G. Tang, 2014: Trend of surface air temperature in eastern China and associated large-scale climate variability over the last 100 years. *J. Climate*, **27**, 4693–4703, https://doi.org/10.1175/JCLI-D-13-00397.1.

Zhong, Z., 2006: A possible cause of a regional climate model's failure in simulating the East Asian summer monsoon. *Geophys. Res. Lett.*, **33**, L24707, https://doi.org/10.1029/2006GL027654.

——, X. Chen, X.-Q. Yang, Y. Ha, and Y. Sun, 2019: The relationship of frequent tropical cyclone activities over the western North Pacific and hot summer days in central-eastern China. *Theor. Appl. Climatol.*, **138**, 1395–1404, https://doi.org/10.1007/s00704-019-02908-7.